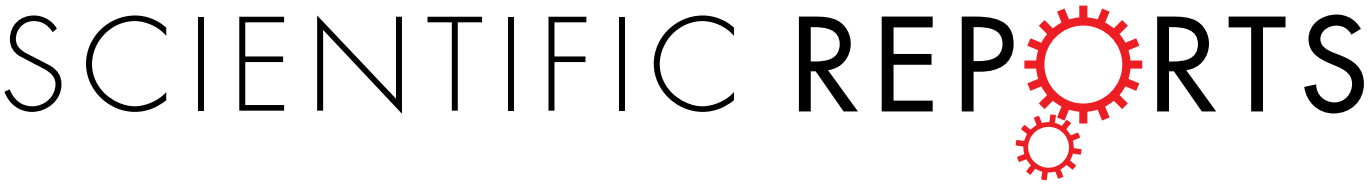

OPEN

Excellent Thermoelectric Properties in monolayer WSe_2 Nanoribbons due to Ultralow Phonon Thermal Conductivity

Received: 26 August 2016
Accepted: 19 December 2016
Published: 25 January 2017

Jue Wang[1], Fang Xie[1], Xuan-Hao Cao[1], Si-Cong An[1], Wu-Xing Zhou[1,2], Li-Ming Tang[1] & Ke-Qiu Chen[1]

By using first-principles calculations combined with the nonequilibrium Green's function method and phonon Boltzmann transport equation, we systematically investigate the influence of chirality, temperature and size on the thermoelectric properties of monolayer WSe_2 nanoribbons. The results show that the armchair WSe_2 nanoribbons have much higher ZT values than zigzag WSe_2 nanoribbons. The ZT values of armchair WSe_2 nanoribbons can reach 1.4 at room temperature, which is about seven times greater than that of zigzag WSe_2 nanoribbons. We also find that the ZT values of WSe_2 nanoribbons increase first and then decrease with the increase of temperature, and reach a maximum value of 2.14 at temperature of 500 K. It is because the total thermal conductance reaches the minimum value at 500 K. Moreover, the impact of width on the thermoelectric properties in WSe_2 nanoribbons is not obvious, the overall trend of ZT value decreases lightly with the increasing temperature. This trend of ZT value originates from the almost constant power factor and growing phonon thermal conductance.

Thermoelectric material, which can directly convert waste heat into electricity and vice versa, have attracted major attentions in recent years due to increasing world energy consumption and decreasing fuel supply[1,2]. Current applications of thermoelectric energy conversion technology, however, are severely hindered by the limited thermoelectric conversion efficiency, which is quantified by a dimensionless thermoelectric figure of merit, defined as $ZT = S^2 \cdot G \cdot T/\kappa$, where S, G, T and κ are Seebeck coefficient, electronic conductance, absolute temperature and thermal conductance (include both the phononic and electronic contributions), respectively. According to the formula, in order to obtain a high ZT, high electronic conductance G, high Seebeck coefficient S, as well as low thermal conductance κ are required. Nevertheless, it is very difficult to modify one quantity independently and keep the other quantities unaffected[3,4]. For instance, the materials with the large electrical conductivity usually have small Seebeck coefficient and large electrical thermal conductivity because of the Wiedemann-Franz relation. Until the 1990 s, Hicks *et al.* theoretically predicated that nanostructuring of materials may improve the thermoelectric properties owing to reduced lattice thermal conductivity caused by phonon-boundary scattering and increased power factor caused by quantum confinement[5]. From then on many kinds of nanostructures materials, such as superlattices[6,7], nanoribbons[8–10], nanowires[11–15], etc, are investigated to seek the high quality thermoelectric materials.

Recent years, transition metal dichalcogenides (TMDCs), as a family of two-dimensional materials, have attracted a lot of attentions due to their potential applications in field-effect transistors, photoelectric devices, thermoelectric devices and so on[16–23]. MoS_2 monolayers, as a typical semiconducting TMDCs, is regarded as a great candidate for thermoelectric applications recently due to the low thermal conductivity and large Seebeck coefficient[24–29]. Nevertheless, WSe_2 monolayers, have a MoS_2-like two-dimensional structure, has much lower thermal conductivity than MoS_2 monolayers[30–31]. Chiritescu *et al.* measured the cross-plane thermal conductivity

[1]Department of Applied Physics, School of Physics and Electronics, Hunan University, Changsha 410082, China. [2]Hunan Province Higher Education Key Laboratory of Modeling and Monitoring on the Near-Earth Electromagnetic Environments, Changsha University of Science and Technology, Changsha 410004, China. Correspondence and requests for materials should be addressed to W.-X.Z. (email: wuxingzhou@hnu.edu.cn) or L.-M.T. (email: lmtang@hnu.edu.cn) or K.-Q.C. (email: keqiuchen@hnu.edu.cn)

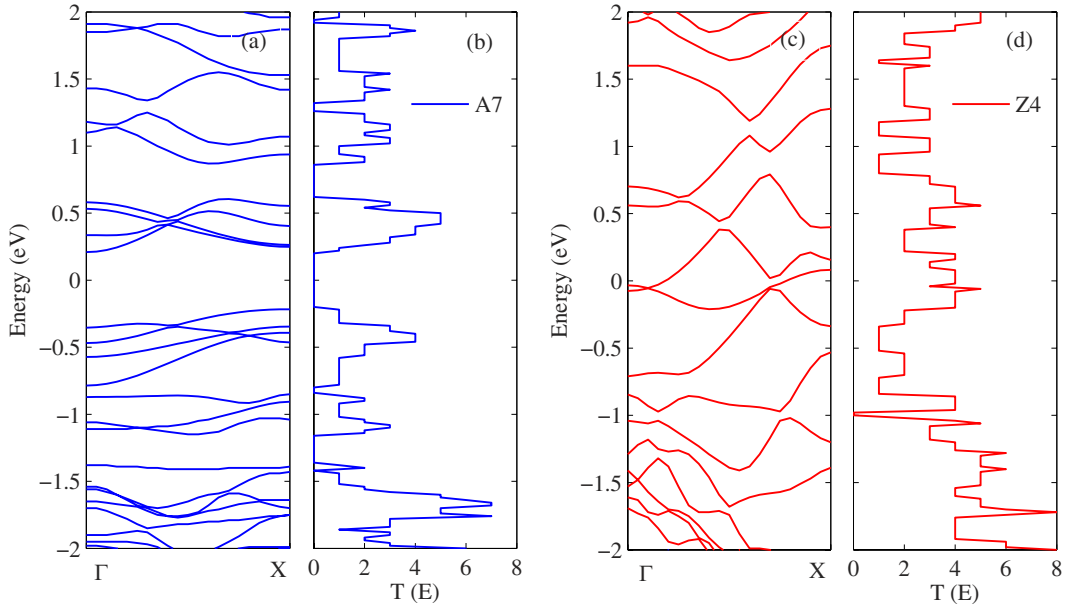

Figure 1. Energy band structure and electron transmission function for (**a**) A7 and (**b**) Z4.

of disordered WSe_2 thin films can be as low as 0.05 W/mK[32], which is the lowest lattice thermal conductivity ever reported for a dense solid. Soon after, Shi *et al.* measured the in-plane lattice thermal conductivity of disordered WSe_2 thin films[33], and found that the in-plane lattice thermal conductivity of the disordered layered WSe_2 thin films is about six times lower than that of compacted single-crystal platelets. Very recently, Zhou *et al.* systematically investigate the lattice thermal conductivity of WSe_2 monolayers by using first-principles calculations combined with the phonon Boltzmann transport equation[34], and found the WSe_2 monolayers have an ultralow thermal conductivity due to the ultralow debye frequency and heavy atom mass. In addition, compared with MoS_2 monolayers, WSe_2 monolayers have a much narrower band gap[35], which can offer a good balance of the electronic conductivity and Seebeck coefficient. Therefore, these researches suggest that the monolayer WSe_2 has great potential in thermoelectric applications.

However, the systematical research on thermoelectric properties of monolayer WSe_2 is still in its infancy. In the present work, we investigate the thermoelectric properties of monolayer WSe_2 systematically by using first-principles calculations combined with the phonon Boltzmann transport equation (PBTE) and nonequilibrium Green's function (NEGF) method. Firstly, we study the chirality effect of monolayer WSe_2 nanoribbons on thermoelectric properties, and find that the armchair WSe_2 nanoribbons have much higher ZT value than zigzag WSe_2 nanoribbons. The ZT value of armchair WSe_2 nanoribbons can reach 1.4 at room temperature, which is about seven times greater than that of zigzag WSe_2 nanoribbons. Moreover, we also discuss the influence of temperature and width on thermoelectric properties in WSe_2 nanoribbons, and find that the ZT value increase first and then decrease with the increase of temperature, and reach a maximum value of 2.14 at temperature of 500 K. However, the impact of width on the thermoelectric properties in WSe_2 nanoribbons is not serious, the overall trend of ZT value decreases lightly with the increasing temperature. These trends of ZT value originate from the competition between power factor and thermal conductivity.

Results

Similar to graphene nanoribbons, WSe_2 nanoribbons also can be zigzag-edged or armchair-edged denoted as A*n* and Z*n*, respectively, where *n* denotes the width of WSe_2 nanoribbons. Firstly, we research the chirality effect of monolayer WSe_2 nanoribbons on thermoelectric properties. For comparison purposes, we chose the A7 and Z4 as the research objects because they have the same width of 1 nm. To understand the thermoelectric transport properties, we first research the electronic transport properties of WSe_2 nanoribbons. Figure 1(a)–(d) show the energy band structure and the electronic transmission function of A7 and Z4, respectively. It is clearly shown that the transmission function of perfect WSe_2 nanoribbons display clear stepwise structure, which indicates that the transport is ballistic, and the electrons from the lead pass through the center region without any scattering. The quantized transmission can also be obtained by counting the numbers of energy bands at any given energy[12]. In addition, it is clearly shown that the A7 is semiconducting, and the Z4 is metallic from Fig. 1(a) and (c). It is interesting that the A7 exhibits a zero transmission window around the Fermi level. It implies that the A7 will have a larger power factor, it is because the Seebeck coefficient is relatively large near the edge of the zero transmission windows.

Based on the electronic transmission function, we calculate the electronic conductance *G*, the Seebeck coefficient *S*, the power factor S^2G and electronic thermal conductance κ_e of A7 and Z4 with different chemical potential at room temperature, as shown in Fig. 2(a)–(d), respectively. In panel (a), we can clearly see that the electronic conductance of Z4 is larger than that of A7 due to the metallic property. In contrast, the Seebeck coefficient is

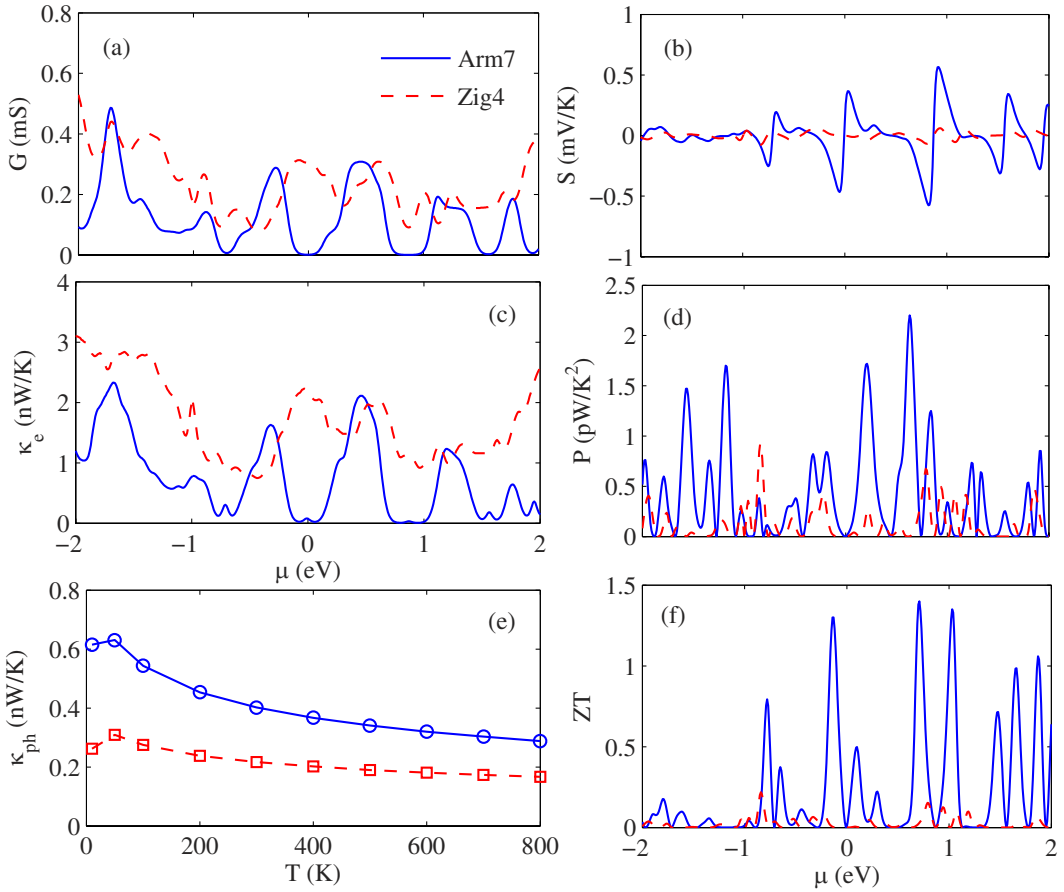

Figure 2. (**a**) Electrical conductance *G*, (**b**) Seebeck coefficient *S*, (**c**) electron thermal conductance κ_e, (**d**) power factor *P*, and (**f**) ZT of A7 and Z4 with different chemical potentials at room temperature. (**e**) Phonon thermal conductance κ_{ph} of A7 and Z4 at different temperatures.

diametrically opposed to electronic conductance, the A7 have a relatively large Seebeck coefficient, as shown in panel (b). This is because the increase of the electrical conductance will decrease the Seebeck coefficient duo to the usual interdependence of the transport parameters[2]. Therefore, the power factor S^2G is depending on the competition between electrical conductance and Seebeck coefficient. In panel (c), we can find that the A7 has a larger power factor than Z4. This result accords closely with our predictions in the part of energy band structure analysis. Panel (d) shows the electronic thermal conductance of the A7 and Z4 at 300 K. As we know, the most important contribution of the thermal conductance comes from phonons in the semiconductor materials and insulation materials, the electronic thermal conductance can be negligible. However, in metallic materials, the electrons have also important contributions to the total thermal conductance. Here, the Z4 has a much large electron conductance than A7 is due to its metallic property. In addition, it is worth noting that the electrons thermal conductance has a similar trend with electronic conductance as shown in Fig. 2(a) and (d), it is because the charge carriers are also heat carriers.

To evaluate the ZT value explicitly, we calculated the temperature dependence of phononic thermal conductance of the A7 and Z4 as shown in Fig. 2(e). We can see that the phononic thermal conductance of A7 and Z4 increase first and then decrease with the increase of temperature. This phenomenon can be understood from the phonon scattering mechanisms. At low temperatures, the Umklapp phonon-phonon scattering is very weak, and a growing number of phonons are excited to participate in thermal transport with the increase of temperature, leading to the phononic thermal conductance increases significantly. However, at high temperature, the Umklapp phonon-phonon scattering is dominant, so the thermal conductance decreases significantly with the increase of temperature. In addition, from Fig. 2(e), we also find that thermal conductance of A7 is significantly higher than that of Z4, the thermal conductance value of A7 is approximately twice than that of Z4. This is because the phonon group velocity along the heat transport direction of A7 is significantly greater than that of Z4[34]. Although the A7 has a higher thermal conductivity than Z4, the ZT of A7 is significantly higher than that of Z4, as shown in Fig. 2(f), the ZT value of A7 can reach 1.4 at room temperature, which is about seven times greater than that of Z4. It is because that the A7 has much higher power factor than Z4 as shown in Fig. 2(c). In addition, it is worth noting that the ZT is heavily depending on the electron chemical potential, we can control the electron chemical potential by chemical doping or electrical gating to get the optimal ZT value[36]. In short, the ZT value is depends on the competition between thermal conductance and power factor.

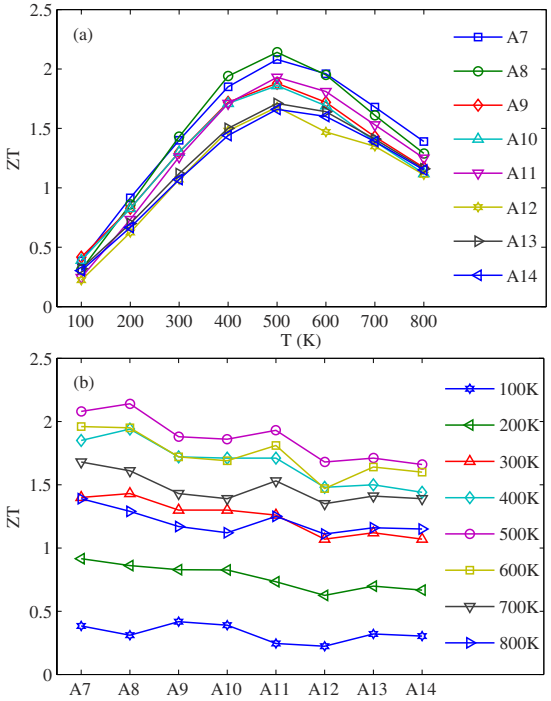

Figure 3. (**a**) The temperature dependence of ZT in monolayer WSe_2 with different widths. (**b**) The width dependence of ZT in monolayer WSe_2 under different temperatures.

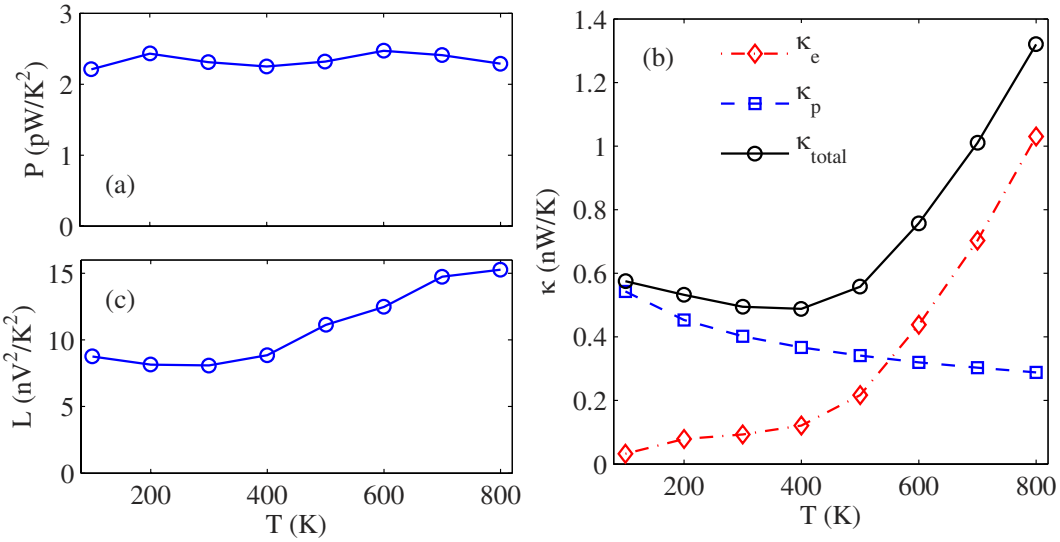

Figure 4. The temperature dependence of (**a**) power factor *P*, (**b**) electron thermal conductance κ_e, Phonon thermal conductance κ_{ph} and total thermal conductance, (**c**) Lorenz number of A7.

In order to further improve the thermoelectric performance of WSe_2 nanoribbons, we study the influences of temperature and size on the thermoelectric properties of armchair WSe_2 nanoribbons. We plot the ZT as a function of the temperature and the width of WSe_2 nanoribbons in Fig. 3(a) and (b), respectively. Obviously, the ZT of WSe_2 nanoribbons increases first with the increasing of temperature, and then decreases, as shown in Fig. 3(a). The ZT value can reach a maximum value of 2.14 at temperature of 500 K. And previous experimental result shows that the structure of WSe_2 is still stable when the temperature is lower than 900K[37]. In addition, from Fig. 3(b) we can find that the influence of width on the thermoelectric properties in WSe_2 nanoribbons is not serious, the overall trend of ZT value decreases lightly with the increasing temperature.

To explain the influence of temperature on the thermoelectric properties of WSe_2 nanoribbons, we plot the power factor and thermal conductance of WSe_2 nanoribbons as a function of temperature in Fig. 4(a) and (b), respectively. Here, the power factor and electronic thermal conductance correspond to the optimal values to

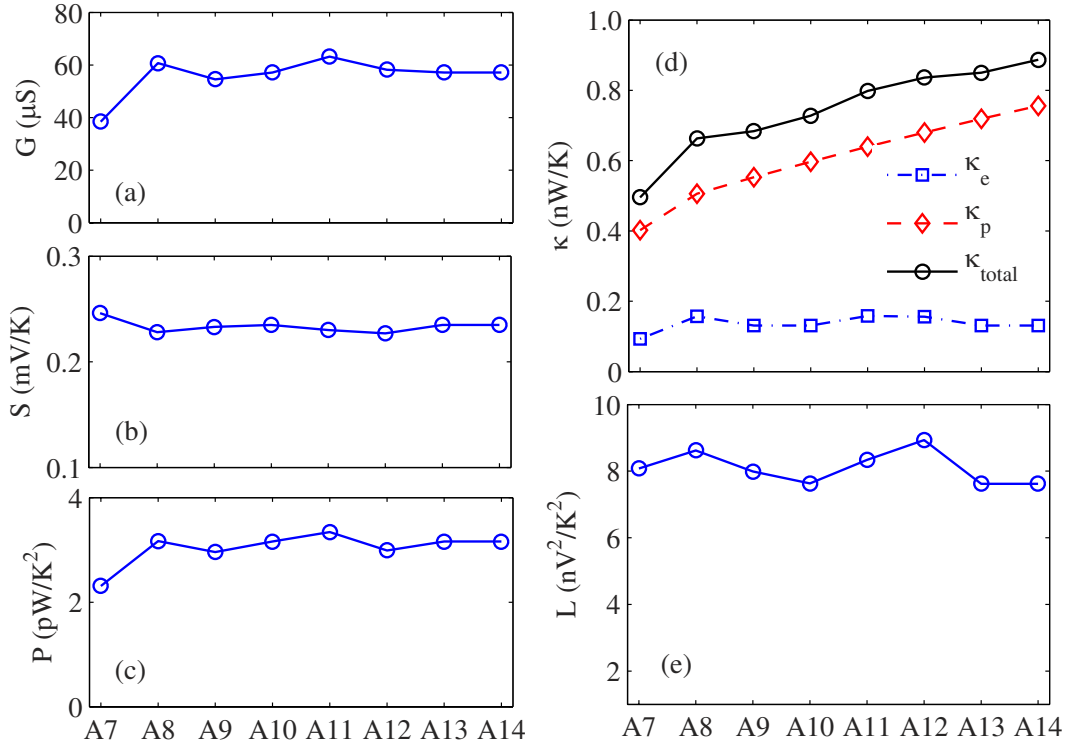

Figure 5. The width dependence of (**a**) Electrical conductance G, (**b**) Seebeck coefficient S, (**c**) power factor *P*, (**d**) electron thermal conductance κ_e, Phonon thermal conductance κ_{ph} and total thermal conductance (**e**) Lorenz number of monolayer WSe_2 nanoribbons at room temperature.

achieve the maximum value of ZT. From Fig. 4(a), we can clearly see that the power factor of WSe_2 nanoribbons almost keeps constant with the increasing of temperature. It is because the influence of temperature on power factor mainly involve the following aspects: On the one hand, the electronic conductance will be increased with the increasing of temperature due to a growing number of electrons can be excited into the conductance band and contribute to the electronic conductance. But on the other hand, the increase of the electrical conductance will decrease the Seebeck coefficient duo to the usual interdependence of the transport parameters. Therefore, the power factor of WSe_2 nanoribbons depends on the competition between electronic conductance and Seebeck coefficient. In addition, the electrons thermal conductance is also increased with the increasing of temperature as shown in Fig. 4(b), because the charge carriers are also heat carriers. But the phononic thermal conductance is decreased with the increasing of temperature due to the enhanced phonon-phonon interaction. As a result the phonons play the dominant role in thermal transport at low temperature, and the electrons play the leading role in thermal transport at high temperature. So the total thermal conductance of WSe_2 nanoribbons decreases with the increasing of temperature, and then increases. This phenomenon results from the competition between electronic thermal conductance and phononic thermal conductance. In short, the influence of temperature on the thermoelectric properties of WSe_2 nanoribbons is depends on the combined effect from electronic conductance, Seebeck coefficient, phononic thermal conductance and electronic thermal conductance. In addition, we also calculate the Lorenz number for the ratio of conductance and thermal conductance of electrons, and find that the Lorenz number is no longer a constant in WSe_2 nanoribbons, but increases obviously as the temperature rises.

In order to further understand the size effect of the thermoelectric properties in WSe_2 nanoribbons, we plot the electronic conductance, the Seebeck coefficient, the power factor, thermal conductance and Lorenz number of WSe_2 nanoribbons as a function of width at 300 K in Fig. 5(a–e), respectively. From Fig. 5(a) and (b), we can find that the electronic conductance and the Seebeck coefficient are almost not changed with increasing the nanoribbons width, causing the optimized power factor is almost constant with the increasing of the width as shown in Fig. 5(c). However, the total thermal conductance of WSe_2 nanoribbons increases significantly as the nanoribbons width increases, as shown in Fig. 5(d). We also find that the phononic thermal conductance of WSe_2 nanoribbons dominate the thermal transport due to the semiconducting properties, and increases significantly with the increasing of nanoribbons width. Nevertheless, the electronic thermal conductance is almost constant. So the increase of total thermal conductance in WSe_2 nanoribbons is due to the increase of phononic thermal conductance, which is because the phonon-boundary scattering is weakened with the increasing of nanoribbons width. In addition, we also find that the Lorenz number does not change much as the size increases from Fig. 5(e). In brief, the light decrease of ZT value with the increasing of nanoribbons width originates from the almost constant power factor and growing phononic thermal conductance.

Discussion

In summary, by using first-principles calculations combined with the nonequilibrium Green's function method and phonon Boltzmann transport equation, we systematically investigate the influence of chirality, temperature and size on the thermoelectric properties of monolayer WSe_2 nanoribbons. The results show that the armchair WSe_2 nanoribbons have much higher ZT value than zigzag WSe_2 nanoribbons. The ZT value of armchair WSe_2 nanoribbons can reach 1.4 at room temperature, which is about seven times greater than that of zigzag WSe_2 nanoribbons. We also find that the ZT value increase first and then decrease with the increase of temperature, and reach a maximum value of 2.14 at temperature of 500 K. It is because the total thermal conductance reaches the minimum value at 500 K. Moreover, we also find the impact of width on the thermoelectric properties in WSe_2 nanoribbons is not serious, the overall trend of ZT value decreases lightly with the increasing temperature. This trend of ZT value originates from the almost constant power factor and growing phononic thermal conductance.

Method

We adopt the density functional theory (DFT) as well as non-equilibrium Green's function method to optimize structure and calculate the electrical transmission, as implemented in Atomistix ToolKit (ATK) software package[38–39]. Since the electron-phonon interaction is very weak in WSe_2 NWs[8,40], in the present work, the electron transport is assumed to travel ballistically. The single-zeta plus polarization (SZP) basis set are employed, and the exchange-correlation potential is described by the local density approximation. The Brillouin zone is sampled with $1 \times 1 \times 100$ Monkhorst-Pack k-mesh, and the cutoff energy is set to 150 Ry. All atomic positions are relaxed until the maximum atomic force becomes smaller than 0.01 eV/A. For electron transport calculation, the retarded Green's function G_r should be obtained firstly,

$$G_r = [\mathrm{ES}_C - \mathrm{H}_C - \Sigma_L^r - \Sigma_R^r]^{-1} \tag{1}$$

Where E is the electron energy, and S_C and H_C are the overlap matrix and Hamiltonian matrix of the center scattering region, respectively. $\Sigma_L^r$and Σ_R^rdenote the self-energy of the left and right semi-infinite leads, which can be calculated as

$$\Sigma_L^r = H_{LC}^{\dagger} g_L^r H_{LC},\ \Sigma_R^r = H_{RC}^{\dagger} g_R^r H_{RC} \tag{2}$$

where $g_L^r$and g_R^r are the retarded surface Green's function of the left and right lead, respectively. Then, according to the Caroli formula, the electron transmission is calculated as

$$\mathrm{T}_e[\omega] = Tr(G^r \Gamma_L G^a \Gamma_R), \tag{3}$$

Where $G^r = (G^a)^{\dagger}$ is the retarded Green function of the central scattering region and $\Gamma_{L(R)}$ represents the coupling interaction with the left (right) semi-infinite lead. Thus, the physical quantities involved in the ZT formula can be obtained by, respectively,

$$G = \mathrm{e}^2 L^{(0)}, \tag{4}$$

$$S = \frac{1}{eT}\frac{L^{(1)}}{L^{(0)}}, \tag{5}$$

$$\kappa_e = \frac{1}{T}\left[L^{(2)} - \frac{(L^{(1)})^2}{L^{(0)}}\right], \tag{6}$$

with

$$L^{(n)} = \frac{2}{h}\int (E-\mu)^n \left[-\frac{\partial f(E,\mu,T)}{\partial E}\right] T_e(E)\, dE, \tag{7}$$

Where $f(E,\mu,T)$is the Fermi-Dirac distribution function at the chemical potential μ and temperature T.

We calculate the lattice thermal conductance by using first-principles calculations combined with the phonon Boltzmann transport equation with relaxation time approximation. The thermal conductivity in branch λ of monolayer WSe_2 in the longitudinal direction of ribbon is derived as

$$\kappa_\lambda = \frac{S}{(2\pi)^2}\int c_{ph} \cdot v_\lambda^2 \cdot \tau_\lambda \cdot d\vec{q} \tag{8}$$

Where λ = TA, LA and ZA[41]. Here we only consider the contribution of three acoustic phonons to the thermal conductivity, because the contribution of optical phonons can be negligible due to the short phonon lifetime and small group velocity[27]. S is the area of the sample, v_λ is the phonon group velocity, which can be calculated as $v_\lambda = d\omega/dq$, ω is the phonon frequency for branch λ at wave vector q. c_{ph} is the volumetric specific heat of each mode, which can be written as

$$c_{ph} = \frac{k_B}{Sd} \cdot \frac{(\hbar\omega/k_BT)^2 e^{\hbar\omega/k_BT}}{(e^{\hbar\omega/k_BT} - 1)^2} \tag{9}$$

Where k_B is the Boltzmann constant, $d = 0.648$ nm is the effective layer thickness of monolayer WSe_2, which is assumed to be the interlayer spacing of bulk WSe_2[42]. $\hbar$ is the reduced Planck constant, and T is the absolute temperature. According to the Matthiessen's rule, the averaged phonon relaxation time $\tau_\lambda$can be given as

$$\tau_\lambda = \frac{1}{1/\tau_\lambda^{\mathrm{U}} + 1/\tau_\lambda^{\mathrm{B}}}, \tag{10}$$

The $1/\tau_\lambda^U$, which is the Umklapp phonon-phonon scattering rate, can be written as[43–44]

$$1/\tau_\lambda^U = \frac{\gamma_\lambda^2 k_B T \omega^2}{M v_\lambda^2 \omega_{D,\lambda}} \tag{11}$$

where γ_λ is the Grüneisen parameter, which characterizes the strength of the Umklapp phonon-phonon scattering. M is the mass of a WSe_2 unit cell, and $\omega_{D,\lambda}$ is the Debye frequency of branch λ. The scattering rate of phonon-boundary scattering can be given as[41]

$$1/\tau_\lambda^B = \frac{v_\lambda}{L}\frac{1-P}{1+P} \tag{12}$$

where L is sample size, and P is the specularity parameter, which is defined as a probability of specular scattering at the boundary. These quantities such as phonon dispersion relation, phonon group velocity and Grüneisen parameter are calculated by using the PHONOPY code combined with Vienna ab-initio simulation Package (VASP) based on the density functional theory[45–47]. The project-augmented wave potential and generalized-gradient approximation exchange-correlation functional are adopted in our calculations[48–49]. The energy cutoff for the plane-wave expansion is set as 400 eV, and a Monkhorst-Pack k-mesh of $12 \times 12 \times 1$ is used to sample the Brillouin zone, with the energy convergence threshold set as 10^{-6} eV. A 18.41 Å vacuum spacing is used to eliminate the interactions emerging from the employed periodic boundary conditions. The structures are fully relaxed until the maximal forces exerted on the atoms are no larger than 10^{-6} eV/Å.

References

1. Majumdar, A. Thermoelectricity in semiconductor nanostructures. *Science* **303,** 777 (2004).
2. Zebarjadi, M., Esfarjani, K., Dresselhaus, M. S., Ren, Z. F. & Chen, G. Perspectives on thermoelectrics: from fundamentals to device applications. *Energy Environ. Sci.* **5,** 5147 (2012).
3. Mahan, G. D., Sales, B. & Sharp, J. Thermoelectric materials: New approaches to an old problem. *Phys. Today* **50,** 42 (1997).
4. Chung, D. Y. *et al.* $CsBi_4Te_6$: A High-Performance Thermoelectric Material for Low-Temperature Applications. *Science* **287,** 1024–1027 (2000).
5. Hicks, L. D. & Dresselhaus, M. S. Thermoelectric figure of merit of a one dimensional conductor. *Phys. Rev. B* **47,** 16631–16634 (1993).
6. Zhou, W. W. *et al.* Multi-Phased Nanoparticles for Enhanced Thermoelectric Properties. *Adv. Mater.* **21,** 3196–3200 (2009).
7. Balandin, A. A. & Lazarenkova, O. L. Mechanism for thermoelectric figure-of merit enhancement in regimented quantum dot superlattices. *Appl. Phys. Lett.* **82,** 3 (2003).
8. Xie, Z. X. *et al.* Enhancement of thermoelectric properties in graphene nanoribbons modulated with stub structures. *Appl. Phys. Lett.* **100,** 183110 (2012).
9. Chen, X. K., Xie, Z. X., Zhou, W.–X., Tang, L.-M. & Chen, K.–Q. Phonon wave interference in graphene and boron nitride superlattice. *Appl. Phys. Lett.* **109,** 023101 (2016).
10. Ouyang, T. *et al.* Thermoelectric properties of gamma-graphyne nanoribbons and nanojunctions. *J. Appl. Phys.* **114,** 073710 (2013).
11. Zhang, G., Zhang, Q., Bui, C. T., Lo, G. Q. & Li, B. Thermoelectric performance of silicon nanowires. *Appl. Phys. Lett.* **94,** 213108 (2009).
12. Zhou, W.-X. & Chen, K.-Q. Enhancement of Thermoelectric Performance by Reducing Phonon Thermal Conductance in Multiple Core-shell Nanowires. *Sci. Rep.* **4,** 7150 (2014).
13. Liu, Y.-Y., Zhou, W.-X. & Chen, K.-Q. Conjunction of standing wave and resonance in asymmetric nanowires: a mechanism for thermal rectification and remote energy accumulation. *Sci. Rep.* **5,** 17525 (2015).
14. Zhou, W.-X., Tan, S., Chen, K.-Q. & Hu, W. Enhancement of thermoelectric performance in InAs nanotubes by tuning quantum confinement effect. *J. Appl. Phys.* **115** 124308 (2014).
15. Takahashi, K. *et al.* Bifunctional thermoelectric tube made of tilted multilayer material as an alternative to standard heat exchangers. *Sci. Rep.* **3,** 1501 (2013).
16. Li, B. *et al.* Synthesis and Transport Properties of Large-Scale Alloy $Co_{0.16}Mo_{0.84}S_2$ Bilayer Nanosheets. *ACS Nano*, **9,** 1257–1262 (2015).
17. Wang, X. *et al.* Enhanced rectification, transport property and photocurrent generation of multilayer $ReSe_2/MoS_2$ p–n heterojunctions. *Nano Res.*, **9,** 507–516 (2016).
18. Wang, Q. H., Kalantar-Zadeh, K., Kis, A., Coleman, J. N. & Strano, M. S. Electronics and optoelectronics of two-dimensional transition metal dichalcogenides. *Nat. Nanotechnol.* **7,** 699 (2012).
19. Butler, S. Z. *et al.* Progress, challenges, and opportunities in two-dimensional materials beyond graphene. *ACS Nano* **7,** 2898 (2013).
20. Chhowalla, M. *et al.* The chemistry of two-dimensional layered transition metal dichalcogenide nanosheets. *Nat. Chem.* **5,** 263 (2013).
21. Sim, S. *et al.* Exciton dynamics in atomically thin MoS_2: Interexcitonic interaction and broadening kinetics. *Phys. Rev. B* **88,** 075434 (2013).
22. Shi, H. *et al.* Exciton dynamics in suspended monolayer and few-Layer MoS_2 2D crystals. *ACS Nano* **7,** 1072 (2013).
23. Kaasbjerg, K., Thygesen, K. S. & Jauho, A.-P. Acoustic phonon limited mobility in two-dimensional semiconductors: Deformation potential and piezoelectric scattering in monolayer MoS_2 from first principles. *Phys. Rev. B* **87,** 235312 (2013).
24. Splendiani, A. *et al.* Emerging photoluminescence in monolayer MoS_2. *Nano Lett.* **10,** 1271–1275 (2010).

25. Cai, Y., Zhang, G. & Zhang, Y.-W. Polarity-reversed robust carrier mobility in monolayer MoS_2 nanoribbons. *J. Am. Chem. Soc.* **136,** 6269 (2014).
26. Buscema, M. *et al.* Large and tunable photothermoelectric effect in single-layer MoS_2. *Nano Lett.* **13,** 358 (2013).
27. Li, W., Carrete, J. & Mingo, N. Thermal conductivity and phonon linewidths of monolayer MoS_2 from first principles. *Appl. Phys. Lett.* **103,** 253103 (2013).
28. Liu, X. J., Zhang, G., Pei, Q. X. & Zhang, Y.-W. Phonon thermal conductivity of monolayer MoS_2 sheet and nanoribbons. *Appl. Phys. Lett.* **103,** 133113 (2013).
29. Jiang, J. W., Park, H. S. & Rabczuk, T. Molecular dynamics simulations of single-layer molybdenum disulphide (MoS_2): Stillinger-Weber parametrization, mechanical properties, and thermal conductivity. *J. Appl. Phys.* **114,** 064307 (2013).
30. Cai, Y. Q., Lan, J. H., Zhang, G. & Zhang, Y.-W. Lattice vibrational modes and phonon thermal conductivity of monolayer MoS_2. *Phys. Rev. B* **89,** 035438 (2014).
31. Yan, R. *et al.* Thermal conductivity of monolayer molybdenum disulfide obtained from temperature-dependent raman spectroscopy. *ACS Nano* **8,** 986 (2014).
32. Chiritescu, C. *et al.* Ultralow thermal conductivity in disordered, layered WSe_2 crystals. *Science* **315,** 351 (2007).
33. Mavrokefalos, A., Nguyen, N. T., Pettes, M. T., Johnson, D. C. & Shi, L. In-plane thermal conductivity of disordered layered WSe_2 and (W)x(WSe_2)y superlattice films. *Appl. Phys. Lett.* **91,** 171912 (2007).
34. Zhou, W.-X. & Chen, K.-Q. First-Principles Determination of Ultralow Thermal Conductivity of monolayer WSe_2. *Sci. Rep*. **5,** 15070 (2015).
35. Huang, W. *et al. Phys. Chem. Chem. Phys.*, **16,** 10866 (2014).
36. Bao, Q. & Loh K. P.Graphene Photonics, Plasmonics, and Broadband Optoelectronic Devices. *ACS Nano* **6,** 3677–3694 (2012).
37. Su, S.-H. *et al.* Controllable synthesis of band-gap-tunable and monolayer transition-metal dichalcogenide alloys. *Front. Energy Res*. **2,** 27 (2014).
38. Taylor, J., Guo, H. & Wang, J. Ab initio modeling of quantum transport properties of molecular electrical devices. *Phys. Rev. B* **63,** 245407 (2001).
39. Brandbyge, M., Mozos, J. L., Ordejon, P., Taylor, J. & Stokbro, K. Densityfunctional method for nonequilibrium electron transport. *Phys. Rev. B* **65,** 165401 (2002).
40. Mazzamuto, F. *et al.* Enhanced thermoelectric properties in graphene nanoribbons by resonant tunneling of electrons. *Phys. Rev. B* **83,** 235426 (2011).
41. Nika, D. L., Pokatilov, E. P., Askerov, A. S. & Balandin, A. A. Phonon thermal conduction in graphene: Role of Umklapp and edge roughness scattering. *Phys. Rev. B* **79,** 155413 (2009).
42. Gu, X. K. & Yang, R. G. Phonon transport in single-layer transition metal dichalcogenides: A first-principles study. *Appl. Phys. Lett.* **105,** 131903 (2014).
43. Morelli, D. T., Heremans, J. P. & Slack, G. A. Estimation of the isotope effect on the lattice thermal conductivity of group IV and group III-V semiconductors. *Phys. Rev. B* **66,** 195304 (2002).
44. Klemens, P. G. Theory of the A-Plane Thermal Conductivity of Graphite. *J. Wide Bandgap Mater*. **7,** 332 (2000).
45. Togo, A., Oba, F. & Tanaka, I. First-principles calculations of the ferroelastic transition between rutile-type and $CaCl_2$-type SiO_2 at high pressures. *Phys. Rev. B* **78,** 134106 (2008).
46. Kresse, G. Ab initio molecular dynamics for liquid metals. *J. Non-Cryst. Solids* **222,** 192–193 (1995).
47. Kresse, G. & Furthmüller, J. Efficiency of ab-initio total energy calculations for metals and semiconductors using a plane-wave basis set. *Comput. Mater. Sci.* **6,** 15 (1996).
48. Kresse, G. & Joubert, D. From ultrasoft pseudopotentials to the projector augmented-wave method. *Phys. Rev. B* **59,** 1758 (1999).
49. Payne, M. C., Teter, M. P., Allan, D. C., Arias, T. A. & Joannopoulos, J. D. Iterative minimization techniques for ab initio total energy calculations: molecular dynamics and conjugate gradients. *Rev. Mod. Phys.* **64,** 1045 (1992).

Acknowledgements

This work was supported by the National Natural Science Foundation of China (Nos. 11274105, 11674090), and by Open Research Fund Program of the Hunan Province Higher Education Key Laboratory of Modeling and Monitoring on the Near-Earth Electromagnetic Environments (No. 20150102), Changsha University of Science & Technology. The work was carried out at National Supercomputer Center in Tianjin, and the calculations were performed on TianHe-1(A).

Author Contributions

K.Q.C., W.X.Z. and L.M.T. conceived this work. J.W., F.X., W.X.Z., X.H.C and S.C.A did the numerical simulations. All authors discussed the results and contributed to the revision of the final manuscript.

Additional Information

Competing financial interests: The authors declare no competing financial interests.

How to cite this article: Wang, J. *et al.* Excellent Thermoelectric Properties in monolayer WSe_2 Nanoribbons due to Ultralow Phonon Thermal Conductivity. *Sci. Rep.* **7**, 41418; doi: 10.1038/srep41418 (2017).

Publisher's note: Springer Nature remains neutral with regard to jurisdictional claims in published maps and institutional affiliations.